Atmos. Chem. Phys. Discuss., 13, 4601–4635, 2013
www.atmos-chem-phys-discuss.net/13/4601/2013/
doi:10.5194/acpd-13-4601-2013

Atmospheric Chemistry and Physics Discussions

Uncertainties in modelling the stratospheric warming following Mt. Pinatubo eruption

F. Arfeuille[1,2], B. P. Luo[1], P. Heckendorn[1], D. Weisenstein[3], J. X. Sheng[1], E. Rozanov[1,4], M. Schraner[5], S. Brönnimann[2], L. W. Thomason[6], and T. Peter[1]

[1]Institute for Atmospheric and Climate Science ETH Zurich, Zurich, Switzerland
[2]Oeschger Center for Climate Change Research and Institute of Geography, University of Bern, Bern, Switzerland
[3]School of Engineering and Applied Science, Harvard University, Cambridge, MA, USA
[4]Physical-Meteorological Observatory/World Radiation Center, Davos, Switzerland
[5]Federal office of Meteorology and Climatology, Meteoswiss, Zürich, Switzerland
[6]NASA Langley Research Center, Hampton, Virginia, USA

Received: 10 December 2012 – Accepted: 1 February 2013 – Published: 18 February 2013

Correspondence to: F. Arfeuille (florian.arfeuille@giub.unibe.ch)

Published by Copernicus Publications on behalf of the European Geosciences Union.

Abstract

In terms of atmospheric impact, the volcanic eruption of Mt. Pinatubo (1991) is the best characterized large eruption on record. We investigate here the stratospheric warming following the Pinatubo eruption derived from SAGE II extinction data including most recent improvements in the processing algorithm and a data filling procedure in the opacity-induced "gap" regions. From these data, which cover wavelengths of 1.024 micrometer and shorter, we derived aerosol size distributions which properly reproduce extinction coefficients at much longer wavelength. This provides a good basis for calculating the absorption of terrestrial infrared radiation and the resulting stratospheric heating. However, we also show that the use of this dataset in the global chemistry-climate model (CCM) SOCOL leads to exaggerated aerosol-induced stratospheric heating compared to observations, even partly larger than the already too high values found by many models in recent general circulation model (GCM) and CCM intercomparisons. This suggests that the overestimation of the stratospheric warming after the Pinatubo eruption arises from deficiencies in the model radiation codes rather than an insufficient observational data basis. Conversely, our approach reduces the infrared absorption in the tropical tropopause region, in better agreement with the post-volcanic temperature record at these altitudes.

1 Introduction

The most recent large tropical volcanic eruption was that of Mt. Pinatubo in June 1991 in the Philippines (15° N). Unlike earlier major volcanic eruptions of the 20th century, Mt. Pinatubo has been relatively well characterised by observations. Several satellite, balloon-borne and ground-based measurements are available during this period (Bluth et al., 1992; Labitzke and McCormick, 1992; McCormick, 1992; Stowe et al., 1992; Thomason, 1992; Minnis et al., 1993; Antuña et al., 2002). However, the peak of the stratospheric aerosol cloud is not well characterized as the observational network was

ACPD
13, 4601–4635, 2013

best established in the Northern Hemisphere and less dense in the tropics and Southern Hemisphere, where a large part of the emitted SO_2 and resulting sulfate aerosols was transported. An additional problem was that for some instruments measuring in the shortwave, the lower stratosphere became opaque. For instance during the first year after the Pinatubo eruption SAGE II measured only above about 23 km altitude at wavelengths of 1.024 µm and shorter. To cope with the regions of missing data, SPARC (2006) provides a "gap-filled" data set spanning the period 1979–2004 using SAGE data amended by measurements from lidar ground stations. This SAGE II gap-filled dataset provides the most complete and accurate (uncertainty around 10 % outside the gap) global optical characterization of the eruption, even if the quality of this dataset in the most perturbed periods is limited, in particular in the tropics with uncertainties in the order of 50 % in the extinction coefficients in the gap region.

There have been several earlier attempts to create a consistent global stratospheric aerosol dataset of the Pinatubo eruption (e.g. Sato et al., 1993; Stenchikov et al., 1998) for climate models. The dataset of Stenchikov et al. (1998) provides spectral extinction coefficients and directly calculated heating rates for modeling studies, while the Sato et al. (1993) "GISS" dataset consists of optical depth data for 0.5 µm wavelength and effective radii in four different altitude ranges and 24 latitude bands derived from SAGE II data. However, these two datasets use outdated versions of the SAGE retrieval algorithm and a very coarse gap-filling procedure (assuming a constant extinction coefficient below 24 km altitude). Furthermore, no systematic comparison with extinction coefficients from HALOE at 3.46 µm and 5.26 µm (Russell et al., 1993; Hervig et al., 1995) or ISAMS at 12.1 µm (Lambert et al., 1997) was performed to verify the applicability for extinction coefficients in the terrestrial IR, which is a requirement for climate simulations. Extinction coefficients of HALOE at 3.46 µm and 5.26 µm are of good quality during the period affected by the Pinatubo eruption (Thomason et al., 2012). ISAMS extinction coefficient uncertainties at 12.1 µm for the equator are in the order of 50 % at 70 hPa and less than 20 % at 45 hPa and above, while for 40° N, uncertainties are less than 25 % below 45 hPa and close to 50 % at 32 hPa (Lambert et al., 1996).

ACPD
13, 4601–4635, 2013

The accuracy of the solar and infrared extinction coefficients in stratospheric aerosol datasets is an important point because large stratospheric volcanic eruptions in the tropics represent major external forcings to the climate system, and many uncertainties remain in their modeling by CCMs/GCMs. Simulations exhibit a large range of responses due to model deficiencies and/or uncertainties in the volcanic forcing. Many GCMs/CCMs overestimate the stratospheric warming after volcanic eruptions and an attribution of this artifact remains difficult because of the large range of optical forcings obtained with different approaches and datasets (SPARC-CCMVal, 2010; Gettelman et al., 2010; Lanzante and Free, 2007).

As noted by Morgenstern (2010), different approaches have been followed among the CCMval-2 (SPARC-CCMVal, 2010) models to represent the volcanic forcing. Some models (CAM3.5, GEOSCOM, LMDZrepro, UMSLIMCAT and UMUKCA-UCAM) do not at all model the heating by the aerosol, while ULAQ REF-B1 uses direct SO_2 injections. A third group derives heating rates consistent with prescribed SAD (Surface Area Density) data (CMAM and WACCM) or use the GISS (Sato et al., 1993) data (AMTRAC3, CCSRNIES, MRI, UMETRAC, UMUKCA-METO). These two methods require assumptions on the size distribution, notably through a fixed distribution width. Some models also use directly the precalculated heating rates from Stenchikov et al. (1998) which are based partly on the Sato et al. (1993) extinction data (E39CA and EMAC). Finally the SOCOL used in CCMval-2 a SAGE II and GISS derived dataset. All these methods produce large differences in the volcanic aerosol optical properties, making it difficult to compare these models against each other.

2 Methods

The most elaborated gap-filled SAGE II 1.024 µm extinction coefficient record is described by SPARC (2006) (hereafter called SAGE_ASAP). The gaps in the SAGE II measurements, mainly caused by opaqueness directly after the Pinatubo eruption, were filled by means of lidar measurements at Mauna Loa in Hawaii, at Camagüey

ACPD
13, 4601–4635, 2013

in Cuba, at Hampton, Virginia (USA) and with backscatter sonde measurements from Lauder, New Zealand. The lidar measurements have been converted to 1.024 µm (SAGE II wavelength) (Antuña et al., 2003). The main aerosol cloud was frequently over Mauna Loa (19.54° N) and Camagüey (21.4° N) and these values are taken for the tropical region. However, due to the fact that the main aerosol cloud was not always located above the two lidar stations, an erroneous seasonality of the aerosol amount might be present in the compiled dataset (SPARC, 2006). The differences between the SAGE V6.0 version used by SPARC (2006) and earlier versions as used by Stenchikov et al. (1998) and Sato et al. (1993) are described in Sect. 3.

To retrieve extinction coefficients (subsequently referred to as "extinctions") in the whole spectral range and subsequently model the stratospheric warming response, the particle size distribution has to be known. During quiescent times the size distribution of stratospheric aerosol is relatively well captured by a simple unimodal lognormal distribution (Wurl et al., 2010). However, after volcanic eruptions a second (and often third) mode are observed, consequently a bimodal (or trimodal) lognormal distribution fits the data better (Deshler et al., 1992). For simplicity and because of patchiness of the data many studies nevertheless use unimodal lognormal distributions (e.g. Kinnison et al., 1994; Russell et al., 1996; Stenchikov et al., 1998; SPARC, 2006). This might be legitimate if one of these modes dominates in terms of surface area density and radiative properties.

In this study we compare four methods to retrieve spectrally resolved optical properties: first, a method with varying effective radii, distribution widths and number densities (called SAGE_4λ hereafter) to find the best fit to the four wavelengths of SAGE_ASAP extinction measurements; second, the method by Stenchikov et al. (1998, called ST98 hereafter) using an older version of the SAGE II data set (from the V5 series); third, a method using an aerosol model (AER-2D, Weisenstein et al. (1997)), where the aerosol size distributions depend directly on microphysical processes and boundary conditions such as SO_2 injection mass and location of injection (7 MT of sulfur injected at 23–25 km in a simulation called AER_7 hereafter); and fourth, the approach

ACPD
13, 4601–4635, 2013

described by Schraner et al. (2008), using SAGE_ASAP and deriving the surface area densities and effective radii based on a Principal Component Analysis using four wavelengths of SAGE II (Thomason et al., 1997b) and assuming a fixed distribution width. Schraner et al. (2008) prescribed the distribution width σ to 1.8 (named SAGE_1.8 below), which is a mean typical value for the last few decades. However, after volcanic eruptions σ can differ substantially from this value. In this study we repeated the calculation for σ equal to 1.2 (SAGE_1.2), which is close to the value for the large particle mode after volcanic eruptions (Deshler et al., 2003) and close to the assumption made by ST98.

Measurements for the sulfur amount injected into the stratosphere are subject to uncertainties. Total uncertainty in the amounts range from 7 to up to 13 Mt S (Lambert et al., 1993; Guo et al., 2004; SPARC, 2006), hence a sensitivity run was performed with AER-2D injecting 9 MT of SO_2 (AER_9). The simulation made for the SPARC ASAP report with 10 MT of SO_2 injected in a broader altitude range (16–29 km), absence of tropospheric washout of aerosols above 10 km (instead of 16 km), and climatological wind fields is also shown (AER_10_ASAP).

Finally, the results from SAGE_4λ and AER_7 are used as input for the CCM SOCOL.v2 (Schraner et al., 2008) to test the radiative response to these optical forcings. The three different SAGE based approaches used to retrieve size distributions are described subsequently. These 3 methods assume unimodal lognormal distributions.

2.1 1st method: SAGE_4λ

The SAGE_4λ method computes single lognormal size distributions, which are described by the total number of particles (N_0), the width of the distribution (standard deviation σ) and the mode radius (r_m):

$$\frac{dN(r)}{dr} = N_0 \frac{e^{-\frac{1}{2}\left[\frac{\ln^2(r/r_m)}{\ln^2\sigma}\right]}}{\sqrt{2\pi} r \ln^2\sigma} \quad (1)$$

ACPD
13, 4601–4635, 2013

where $dN(r)$ is the number concentration of particles in the interval with radius $\in [r, r + dr]$. From the size distribution and H_2SO_4 wt% (calculated using 1991 annual mean ERA-interim relative humidity), the spectrally resolved optical properties can be calculated by means of Mie theory (Mie, 1908).

In this approach, the four wavelengths (385, 452, 525 and 1024 nm) of the SAGE II data are used when available. A similar approach as SAGE_4λ was used in Bingen et al. (2003) showing good results. In a first step, the mode radius r_m, distribution width σ and the number density N_0 are left practically unconstrained for each latitude/altitude point in time ($\sigma \in [1.2, 2.6]$, $r_m \in [0.015\,\mu m, 0.5\,\mu m]$, and $N_0 \in [0.5\,cm^{-3}, 1000\,cm^{-3}]$). For each individual location and time the best set of parameters, minimizing the difference to the SAGE II extinctions at its 4 wavelengths, is obtained. The extinction at each SAGE wavelength is weighted by its standard deviation when available from the SAGE_ASAP dataset, giving more weight to more precise measurements. As the 4 wavelengths of SAGE do not represent entirely independent pieces of information, multiple solutions are possible for the 3 parameters. Thus, a second step is needed in order to avoid unphysical abrupt changes in the aerosol radii in space and time. Therefore, the effective radius r_{eff} is calculated out of the previously fitted r_m and σ parameters:

$$r_{eff} = r_m e^{\frac{5}{2}\ln^2\sigma} \quad (2)$$

The scatterplot of r_{eff} as function of the extinction coefficient at 1.024 µm is then computed and the median values of the scattered r_{eff} are taken for each extinction value (see Fig. 1). The calculated median values are then used in the fitting process and the σ and number density are fitted again to minimize the differences to the SAGE observations. The r_{eff} instead of the mode radius is used for the correlation to the extinction at 1.024 µm because it includes informations about the distribution width σ. The correlation of the extinction at 1.024 µm with r_{eff} is hence more robust as it contains more information about the particles size distributions. The SAD is the principle quantity we are interested in. SAD is not used for the correlation because in the second step the

ACPD
13, 4601–4635, 2013

number density and the width σ are fitted so that the SAGE II extinctions are matched. The fitting of the number density and σ thus allows to reach good agreement with the extinctions at all SAGE wavelengths. Furthermore, the calculated extinctions show good agreement with ISAMS and HALOE data (extinctions at longer wavelengths, see Sect. 4). The resulting size distribution and SAD are then consistent with observations from SAGE to ISAMS wavelengths. This procedure eliminates the unphysical ambiguities mentioned above.

One exception to this second step was made to describe the tropical lower stratosphere in the first months after the eruption. Indeed in the lower stratosphere the coagulation rate is low due to a small diffusion coefficient of aerosol particles (high pressure, low temperature). Hence, in the volcanic aerosol nucleation plume, the new volcanic aerosols formed after the eruption do not coagulate quickly and the relationship between extinctions and effective radii breaks down. For that reason, until September 1991 the aerosol radius in the tropical lower stratosphere can freely adjust so that available SAGE wavelenghts are matched. This leads to smaller (but more numerous) aerosols (see Figs. 3a and 4b and description in Sect. 4 below) and hence reduces the aerosol absorption in this region.

In the gap-filled region, only the extinction at 1.024 µm is available and there is not enough information to fit the size distribution parameters. Therefore, σ is fixed to 1.2 (close to the value for the large mode after volcanic eruptions). The r_{eff} is then obtained through its correlation with the extinction, i.e. the same relationship as in the gap-free regions, and finally the number density is fitted to match the 1.024 µm extinction.

2.2 2nd method: ST98

ST98 used effective radii retrieved from CLAES and ISAMS extinction measurements proposed by Grainger et al. (1995) and Lambert et al. (1997). In general there is a good correspondence to effective radii retrieved from SAGE II. They assumed a fixed distribution width of $\sigma = 1.25$. In a first step ST98 calculated the extinction for a number density of one particle per cm^3 and in a second step scaled the number density to

ACPD
13, 4601–4635, 2013

fit the extinction at 1.024 µm with SAGE II measurements. ST98 use an old SAGE II data set (Russell et al., 1996) with an older satellite retrieval procedure (SAGEv5.9 or similar) and a very simplified gap-filling approach (the last measured SAGE II value in vicinity is taken to fill the gap). ST98 used $\sigma = 1.25$ because this distribution width matched best with CLAES optical depth at 2.6 µm. The optical properties are then calculated with Mie theorie assuming H_2SO_4 solution droplets of 70 %. It should be noted that the retrieval of SAGE version V5.9 is significantly different from SAGE V6.0 and higher, and should no longer be used. Conversely, differences in the aerosols from SAGE V6.0 to V7 (recently published) are minor. See Sect. 3 below for details.

2.3 3rd method: SAGE_1.8 and SAGE_1.2

Based on a principal component analysis using four wavelength of SAGE II Thomason et al. (1997b) found the following relationship between the extinctions at 1.024 µm and the surface area density. SAD:

$$\mathrm{SAD} = \begin{cases} 425 \times k^{0.68} & \text{for } k < 4 \times 10^{-3} \\ 1223 \times k^{0.875} & \text{for } 4 \times 10^{-3} < k < 2 \times 10^{-2} \\ 2000 \times k & \text{for } 2 \times 10^{-2} < k \end{cases} \quad (3)$$

where k is the extinction coefficient at 1.024 µm in km^{-1} and SAD is in $\mu\mathrm{m}^2\,\mathrm{cm}^{-3}$. This relationship is based on the assumption that the wavelength dependence of the extinction is stable for different aerosol extinctions. This assumption is justified for most cases. For SAD around 0.1 $\mu\mathrm{m}^2\,\mathrm{cm}^{-3}$ the uncertainty ranges within ±30 %, for SAD greater than 10 $\mu\mathrm{m}^2\,\mathrm{cm}^{-3}$ within ±15 % (Thomason et al., 1997b). However, after the Mt. Pinatubo eruption this relationship differs significantly in the tropical lower stratosphere from the real SAD. This deviation is caused by conjunction of small aerosol size and large extinction after the injection of large amounts of small aerosol following the eruption (SPARC, 2006, Chapter 4, pp. 138 ff). Unfortunately there are no aerosol size distribution measurements in the tropics during that time, for example using the

ACPD
13, 4601–4635, 2013

OPC (Optical Particle Counter), but it is conceivable that due to changes in the size distribution in post-volcanic times this relationship can lead to significant errors.

Similarly to the SAD the effective radius r_{eff} can be retrieved from the extinction at 1.024 µm as following:

$$r_{\text{eff}} = \begin{cases} 0.0303 \times [\ln(k) + 11.515] + 0.16 & \text{for } 1 \times 10^{-5} < k < 3.0 \times 10^{-4} \\ 0.15 \times \exp(0.04916 \times [\ln(k) + 11.513]^2) & \text{for } 3.0 \times 10^{-4} < k < 1.8 \times 10^{-3} \\ 0.55 & \text{for } 1.8 \times 10^{-3} < k \end{cases} \quad (4)$$

Schraner et al. (2008) assumed $\sigma = 1.8$ (SAGE_1.8), which is a mean value for the last few decades. However, after volcanic eruptions σ can differ substantially from this value. Following Stenchikov et al. (1998) we repeated the calculation for $\sigma = 1.2$ (SAGE_1.2). The extinction is very sensitive to σ. For the same aerosol mass, if σ is large, there are fewer but bigger particles. This affects the radiative properties of the aerosol layer: for the same total mass, smaller particles scatter shortwave radiation more efficiently, but absorb longwave radiation almost to the same degree as larger particles. The number density N_0 is finally calculated from the SAD, σ, and r_{eff}.

The main difference between the SAGE_1.8, SAGE_1.2, SAGE_4λ and ST98 approaches is the estimation of the particle size distribution. SAGE_1.8 and SAGE_1.2 follow the approach of SAD conservation from a Principal Component Analysis (Thomason et al., 1997a), whereas SAGE_4λ and ST98 derive size distributions such that the extinctions at the SAGE wavelength(s) match the observations best.

3 Differences between pre and post version 6 SAGE II aerosol products

SAGE II began operations in 1984 when aerosol loading was still enhanced above background levels by the 1982 eruption by El Chichón. The aerosol levels were further enhanced by the eruptions of Nevado del Ruiz in 1985 and Nyamuragira in 1986. Despite these enhancements, the total levels of aerosol opacity along the SAGE II

ACPD
13, 4601–4635, 2013

measurement line-of-sight (LOS) geometry remained well below the level at which transmission drops below measureable levels (about an optical depth of 7 along the path between the spacecraft and the Sun) and extinction profiles were made into the upper troposphere throughout this period. After the eruption of Pinatubo in 1991, the LOS optical depth was significantly above 7 and remained so well into 1993 particularly in the tropics. As a result most profiles were terminated in the lower stratosphere even as high as 25 km in the first few months after the eruption. Nominally, both the version 5 series of SAGE II products and version 6 series reflect these facts. However, it became apparent to the SAGE II algorithm team that the version 5 series had serious deficiencies which required the algorithm developments that eventually produced V6.0. The most important of the deficiencies was associated with normalization (producing transmission) and altitude registration. SAGE II observes the Sun through the limb of the atmosphere, scanning across the solar disk normal to the surface of the Earth using a mirror, and uses observations made above the atmosphere to convert observations to transmission and eventually profiles of ozone, NO_2, water vapor and aerosol extinction coefficient at 4 wavelengths. Under most conditions, SAGE II uses observations of the upper and lower edges of the Sun to locate the position of measurements on the Sun and the location of the tangent point in the atmosphere. The location on the Sun is important to converting observations to transmission while locating events in the atmosphere is crucial to accurate altitude registration of the data. The rate of motion of the scan mirror across the Sun is estimated from the times the edges of the Sun are observed. In cases where optically dense layers are observed, the lower edge of the Sun becomes unobservable and both the Sun position and the position are inferred using only the upper edge of the Sun and a prediction of the rate of motion of the scan mirror. The SAGE II algorithm team observed that the algorithms used prior to V6.0 did a poor job of estimating this scan rate and as a result the position of points in which the lower of edge of the Sun was obscured had significant errors in both location on the Sun and in the atmosphere. The effect was generally a smearing of the thick parts of the profile to higher altitudes (above where it was actually observed) and below the point at

ACPD
13, 4601–4635, 2013

which profiles should have terminated. This was true for clouds as well as the Pinatubo aerosol layer. Versions 6.0 and later employ a substantially improved single Sun-edge algorithm and, as such, exhibit a far superior performance around optically thick layers. For instance, in V5.93 clouds were frequently observed above the tropopause but in V6.0 and later, with the exception of polar stratospheric clouds, cloud frequency above the tropopause is effectively zero. For Pinatubo, the observed top of the aerosol layer is much sharper and is no longer smeared over multiple kilometers. As a result, with the release of V6.0 in 2000, the SAGE II algorithm team considered versions prior to V6.0 to be so deficient that these versions were withdrawn from circulation and they strongly recommended that they no longer be employed for any application. Figure 2 demonstrates the differences in these profiles showing a comparison of V5.93 and V6.0 zonally-averaged aerosol extinction in the tropics in August 1991. We can see the much higher termination of the SAGE II V5.93 extinctions compared to V6.0. The Russell et al. (1996) and Sato et al. (1993) extinction data sets (subsequently used by Stenchikov et al., 1998) are built using V5.93 (or similar version) with all its clear defects. However, the data quality issues are exacerbated from this point by the method in which events which terminate above the tropopause (so called saturated events) are extended to the tropopause. In this data set, the last observation (which is significantly compromised) is used at all altitudes down to the tropopause and not otherwise constrained by any observation. The ASAP data set is a significant improvement over that available in 1998. Foremost, it is based on V6.2, a far superior version than anything prior to V6.0, and it also uses a collection of corroborative data, primarily ground- and aircraft-based lidar observations, to fill the observations lost to the extreme opacity of the stratosphere in 1991 through 1993 (SPARC, 2006). While these observations are converted to 1020 nm extinction using an uncertain extinction-to-backscatter ratio, converting to bulk properties (e.g. SAD) is based on statistical relationships inferred from the SAGE II multichannel data and corroborative data in the tropics is scarce, there can be no doubt that this approach is many times more robust than that used in the earlier data set.

ACPD
13, 4601–4635, 2013

The ST98 extinctions are based on 5 km resolution optical depths values from Sato et al. (1993), as seen in Fig. 2. SAGE V5.93 shows larger values (maybe due to changes in altitude resolution from extinctions computed by Sato et al., 1993; Russell et al., 1996) but shows clearly the high altitude of termination from where data was filled by downward extrapolation. This leads the pre-SAGE 6.0 datasets to miss the extinction peak around 40 hPa and to overestimate the extinction below 70 hPa due to lack of satellite data.

4 Results

The extinction, single scattering albedo and asymmetry factor at wavelengths covering the whole spectral range are the key parameters to model the radiative impact of stratospheric aerosols. These quantities are calculated by means of Mie theory (Mie, 1908) for spherical dielectric aerosol particles, using refractive indices measured by Luo et al. (1996) and Biermann et al. (2000), temperature and H_2SO_4 wt% (calculated based on 1991 annual mean ERA-interim relative humidities), applied to the retrieved size distributions.

4.1 Size distributions

Figure 3 shows size distributions derived from SAGE_4λ and from the AER-2D model runs for a 7 MT eruption (AER_7) and volcanically quiescent conditions (Background). Furthermore, it shows a comparison with optical particle counter (OPC) measurements from Laramie, Wyoming (Rosen, 1964; Deshler et al., 1992). The AER-derived size distributions at the equator in August 1991 (Fig. 3a) show the development of the volcanic mode and a shift of the background mode to larger radii. The SAGE_4λ background size distribution (taken from January 1991) shows less small aerosols compared to the AER background simulation. In August 1991 at 64 hPa, the SAGE_4λ approach including the modification in the early volcanic plume (as discussed in the Sect. 2) shows

ACPD
13, 4601–4635, 2013

a wide unimodal distribution with a large number of small aerosols, while this is not the case for the SAGE_4λ distribution not incorporating this special modification. The modification allows the SAGE_4λ method to capture the high 0.525 µm to 1.024 µm extinction ratio below 60 hPa right after the eruption (Fig. 4b). This high ratio is the result of high particle number densities as a consequence of slow coagulation due to a limited diffusion coefficient of aerosol particles (high pressure, low temperature). Figure 3b shows a comparison with OPC measurements from Laramie (41° N) at 64 hPa for January 1992. The SAGE_4λ approach covers the two modes of the observed distribution, but exhibits fewer aerosols below 0.35 µm. This deficiency does not significantly affect the later retrievals of longwave extinction and heating rates, because the SAGE_4λ result provides a good approximation for the large particles and hence for aerosol volume density. The AER_7 simulation captures well the high end of the distribution but underestimates the radius of the aerosols in the background mode, possibly due to a too rapid latitudinal distribution in the 2-D model.

From these size distributions, extinctions are computed for short and long wavelengths and compared to measurements from SAGE II at 1.024 µm, HALOE at 3.46 µm and 5.26 µm, and ISAMS at 12.1 µm.

4.2 Shortwave extinctions

SAGE_4λ shows perfect agreement with SAGE_ASAP at 1.024 µm as shown in Figs. 5a and 6a at the equator. This illustrates the accuracy of SAGE_4λ in matching the various wavelengths of SAGE_ASAP by adjusting the number density and distribution width of the aerosols. ST98, with retrieval based on old data (Russell et al., 1996), is less than half of SAGE_ASAP 1.024 µm measurements at 40 hPa in 1991 (Fig. 5a). Above 20 hPa and below 60 hPa at the equator, ST98 overestimates SAGE_ASAP data (Fig. 6a). Accordingly, heating rate calculations in GCMs and CCMs based on ST98 use a data set that significantly underestimates the extinction at 1.024 µm in the tropical stratosphere in the 50–30 hPa range and overestimates it below.

ACPD
13, 4601–4635, 2013

The AER simulations significantly overestimate the extinction at the equator when compared to SAGE_ASAP. However, in the extra-tropics, AER_7 results are generally in very good agreement with the observations (Fig. 7a, b). At this latitudes, SAGE_4λ and ST98 show similar values, in agreement with SAGE_ASAP data.

The profiles of Fig. 6a show that SAGE_1.8 and especially SAGE_1.2 overestimate the extinctions at 1.024 µm at all altitudes.

4.3 Longwave extinctions

All the SAGE derived methods are based on extinctions at short wavelengths ($\lambda \leq$ 1.024 µm). The longwave radiations peak are mainly responsible for the in-situ heating. Whether the retrieved aerosol size distribution can represent the extinctions at these long wavelengths is a critical question. In the following section, we compare the calculated results with satellite measurements at infrared wavelengths.

The extinctions at 3.46 µm, 5.26 µm and 12.1 µm provide information on the aerosol absorption in the terrestrial IR which is mostly responsible for the stratospheric warming after an eruption. At 40 hPa (Fig. 5b) SAGE_4λ is in good agreement with available measurements at the equator, while ST98 exhibits too low values and AER_7 overestimates the extinction until spring 1992. However, at mid-latitudes results from AER_7 at 12.1 µm agree better with observations, while ST98 underestimates the extinctions at 12.1 µm compared to ISAMS observations (Fig. 7c, d) despite showing accurate extinctions at 1.024 µm (Fig. 7a, b). This indicates a too high 1.024 µm to 12.1 µm extinction ratio in ST98. In December 1991 at 40 hPa, large extinctions are displayed in SAGE_1.8 and SAGE_1.2 which are significantly larger than the ISAMS values (Fig. 6b). Conversely, at 30 hPa, SAGE_1.8, SAGE_1.2 and SAGE_4λ slightly underestimate the extinctions.

The SAGE_4λ calculation shows a reasonable agreement with the data, especially in the level of high extinction above 40 hPa, while ST98 results again are less than half the measurements, approaching the observations only below 70 hPa. The low extinctions at 12.1 µm from the ST98 arise both from its use of an outdated version of the SAGE

ACPD
13, 4601–4635, 2013

retrieval algorithm and gap-filling and from a too high 1.024 µm to IR extinction ratio compared with observation (see Fig. 4c, d).

Compared to HALOE data, SAGE_4λ also show good agreement after the eruption, with differences to the HALOE extinctions at 3.46 µm mostly below 25% right after the eruption at the equator and mid-latitudes (Fig. 8). The 30–40° N extinctions at 5.26 µm 6 months after the eruption are also comparable to HALOE observation for SAGE_4λ, despite an overestimation around 40 hPa (Fig. 10). This overestimation at 40 hPa is also seen when compared to ISAMS measurements (Fig. 6b). SAGE_1.2 and especially SAGE_1.8 show mostly too large extinctions. The ST98 extinctions at 5.26 µm show a similar too low altitudinal distribution compared to observations as its 12.1 µm wavelength did. HALOE values are larger than ST98 between 70 hPa and 40 hPa (twice larger at 60 hPa), and much lower below.

The measurements at far-infrared (HALOE and ISAMS) were not used in the retrieval procedure of the SAGE_4λ size distributions. The good agreement between ISAMS/HALOE and SAGE_4λ suggests that:

1. The assumed unimode lognormal size distribution is capable to describe both extinction coefficients in the short wavelength range but also in the long wavelength range, despite it may deviate from the actual size distribution.

2. The derived lognormal size distributions based on data only at SAGE wavelengths are reasonable and allow us to calculate radiative properties at far-infrared.

The sensitivity simulations performed with the AER model show the influence of the injection mass on the extinction values. Clearly, the AER_9 and AER_10_ASAP simulations yield too high extinctions. The 7 Mt simulation (AER_7) performs the best but still overestimates extinctions at the equator. Figure 6a, b shows that 6 months after the eruption, AER simulations generally show too large values for extinctions at 1.024 µm and 12.6 µm at the equator. Below 70 hPa, the extinction profiles at 12.6 µm of AER_7 and AER_9 are largely consistent with observations, while AER_10_ASAP shows a significant extinction overestimation at low altitudes due mainly to the absence of washout

ACPD
13, 4601–4635, 2013

above 10 km in this simulation. At mid-latitudes, AER_7 and AER_9 values are close to observations, AER_10_ASAP still being an outlier (Fig. 9). At 5.26 µm, the AER simulation AER_10_ASAP is again an outlier compared to HALOE data, while AER_9 extinctions are reasonable but showing a too broad altitude distribution (Fig. 10).

4.4 Stratospheric temperatures

Simulations with the CCM SOCOL.v2 (Schraner et al., 2008) were carried out to test the stratospheric response to the SAGE_4λ and AER_7 scenarios. The GCM part of SOCOL is based on ECHAM-4 using the ECHAM-4 radiation code. For the radiative transfer calculations spectral extinctions, single scattering albedos, asymmetry factors (as well as the surface area densities for heterogeneous chemistry calculations) directly derived from the described methods were provided as boundary conditions to SOCOL. In Fig. 11, these SOCOL results are compared to the ERA-40 reanalysis and to values from different general circulation models (GCM) as shown in Lanzante and Free (2007) and from chemistry climate models (CCM) as shown in Eyring et al. (2006); SPARC-CCMVal (2010).

The stratospheric warming after the eruption is in general overestimated. SAGE_4λ shows a bias between 1 K in fall 1991 to 3 K in spring 1992 in the tropics at 50 hPa compared to ERA40 data (Fig. 11a). Compared to GCM studies using the Sato et al. (1993) or Ammann et al. (2003) datasets (Lanzante and Free, 2007), the SAGE_4λ is in the high range of the tropical warming overestimation, while AER_7 exhibits even larger values. In the same way, the global average temperature increase at 50 hPa from the SAGE_4λ experiment is too high by 1.5 K in spring 1992 (Fig. 11b). The AER results are higher than the SAGE_4λ calculations for the end of 1991. The global average temperature increase at 70 hPa shows similar characteristics (Fig. 11d). Compared to CCM studies using heating rates from Stenchikov et al. (1998) or derived from SPARC (2006) surface area density data or Sato et al. (1993) extinction, SAGE_4λ lies in the high range of their estimations at 50 hPa and 70 hPa. In the tropical tropopause region (100 hPa), SAGE_4λ diverges from ERA40 anomalies in late 1991 (Fig. 11c). At

ACPD
13, 4601–4635, 2013

100 hPa, the SAGE_4λ approach leads to a clear improvement compared to the GCM studies, while AER_7 is inside the range of their results.

5 Conclusions

The volcanic eruption of Mt. Pinatubo in June 1991 is the best documented large eruption on record, however lack of measurements in the tropics in the first months after the eruption due to optical saturation limits the quality of the data. GCMs and CCMs show important variations in lower stratospheric temperatures following the Pinatubo eruption with a tendency to overestimate the warming (SPARC-CCMVal, 2010; Gettelman et al., 2010; Lanzante and Free, 2007). CCMs which implement the aerosol heating using Stenchikov et al. (1998) precalculated heating rates overestimate the stratospheric warming only slightly, but this apparent agreement is fortuitous, because the ST98 dataset present too low IR extinctions compared to measurements. This underestimation of the infrared extinctions is due to the use of an outdated version of the SAGE retrieval algorithm and gap-filling (and also further due to a too high 1 µm to IR extinction ratio). GCMs, which in the past have used the Sato et al. (1993) GISS dataset (also based on an outdated version of SAGE II) and a fixed distribution width tend to overestimate the warming, as do CCMs using heating rates derived from SPARC (2006) surface area density data (Morgenstern, 2010; Lanzante and Free, 2007). The results from these approaches will depend on the choice of the aerosol distribution width, although using a fixed width of either 1.8 or 1.2 together with SPARC (2006) SAD and effective radii did not lead to satisfactory IR extinctions in our study.

An erroneous prescription of the volcanic aerosol forcing can lead to a false error attribution to the radiation scheme of a specific model or hide a bias by compensating errors in the external forcing and the radiation scheme. Therefore, extinctions or heating rates derived from the Stenchikov et al. (1998) or Sato et al. (1993) datasets should no longer be used. We investigated in this study the influence of the improvement of the general satellite extinction processing algorithm and of the gap filling (SPARC,

ACPD
13, 4601–4635, 2013

2006) on the stratospheric warming after the Pinatubo eruption. Using the state-of-the-art SAGE II retrieval algorithm, we derived aerosol size distributions with different methods to calculate spectrally resolved optical properties for the Pinatubo eruption and tested the accuracy of the infrared extinctions compared to ISAMS measurements. The dataset produced using a fit to the four wavelengths of SAGE II (SAGE_4λ) shows a good agreement with extinction profiles and evolutions of both SAGE II visible/near infrared wavelengths and IR measurements from HALOE at 3.46 µm and 5.26 µm and ISAMS at 12.1 µm while the dataset from Stenchikov et al. (1998) displays too low extinctions above 20 km. The use of SPARC (2006) surface area density data and a fixed distribution width (SAGE_1.8, SAGE_1.2) to infer the optical parameters leads to somewhat too large extinctions in the infrared compared to measurements. Results using the microphysical aerosol model AER to generate the aerosol size distributions reveal a clear overestimation of the extinctions at the equator (even though the AER model was found to be one of the most successful aerosol models in SPARC, 2006) but a general good agreement in the extra-tropics.

Using the SAGE_4λ data to simulate the Pinatubo eruption in the CCM SOCOL leads to a significant overestimation of the tropical stratospheric temperatures, by up to 3 K at 50 hPa, but a generally good agreement at 100 hPa.

For GCM and CCM simulations using volcanic forcings with longwave extinctions for the Pinatubo eruption lower than found in this study for the aerosol peak around 40–50 hPa, we argue that the stratospheric temperature increase overestimation often present in these models is unlikely due to an error in the volcanic aerosol forcing data, and could even be amplified by using a dataset closer to the SAGE_ASAP, HALOE and ISAMS observations. Rather, the cause of this problem is likely due to constraints in the radiation codes of the respective models. Conversely, the warming at the tropical tropopause could be reduced by using the new SAGE_ASAP data and an appropriate size distribution retrieval. Finally, our study shows that the use of the surface area density and effective radius information from a principal component analysis (as done

ACPD
13, 4601–4635, 2013

in SPARC, 2006) combined with a fixed distribution width of either 1.8 or even 1.2 leads to an overestimation of the infrared extinctions and therefore should be avoided.

Acknowledgements. We would like to acknowledge funding from the Cogito foundation and from the Department of Environmental Science of ETH Zurich. Discussions with S. Fueglistaler in the early phase of this work are gratefully acknowledged.

References

Ammann, C. M., Meehl, G. A., Washington, W. M., and Zender, C. S.: A monthly and latitudinally varying volcanic forcing dataset in simulations of 20th century climate, Geophys. Res. Lett., 30, 1657, doi:10.1029/2003GL016875, 2003. 4617

Antuña, J. C., Robock, A., Stenchikov, G. L., Thomason, L. W., and Barnes, J. E.: Lidar validation of SAGE II aerosol measurements after the 1991 Mount Pinatubo eruption, J. Geophys. Res. Atm., 107, 4194, doi:10.1029/2001JD001441, 2002. 4602

Antuña, J. C., Robock, A., Stenchikov, G., Zhou, J., David, C., Barnes, J., and Thomason, L.: Spatial and temporal variability of the stratospheric aerosol cloud produced by the 1991 Mount Pinatubo eruption, J. Geophys. Res. Atm, 108, 4624, doi:10.1029/2003JD003722, 2003. 4605

Biermann, U. M., Luo, B. P., and Peter, T.: Absorption spectra and optical constants of binary and ternary solutions of H_2SO_4, HNO_3, and H_2O in the mid infrared at atmospheric temperatures, J. Phys. Chem. A, 104, 783–793, 2000. 4613

Bingen, C., Vanhellemont, F., and Fussen, D.: A new regularized inversion method for the retrieval of stratospheric aerosol size distributions applied to 16 years of SAGE II data (1984–2000): method, results and validation, Ann. Geophys., 21, 797–804, doi:10.5194/angeo-21-797-2003, 2003. 4607

Bluth, G. J. S., Doiron, S. D., Schnetzler, C. C., Krueger, A. J., and Walter, L. S.: Global tracking of the SO_2 clouds from the June, 1991 Mount-Pinatubo eruptions, Geophys. Res. Lett., 19, 151–154, 1992. 4602

Deshler, T., Hoffman, D. J., Johnson, B. J., and Rozier, W.: Balloon-borne measurements of the Pinatubo aerosol size-distribution and volatitily at Laramie, Wyoming, during summer of 1991, Geophys. Res. Lett., 19, 199–202, 1992. 4605, 4613

ACPD
13, 4601–4635, 2013

Deshler, T., Hervig, M. E., Hofmann, D. J., Rosen, J. M., and Liley, J. B.: Thirty years of in situ stratospheric aerosol size distribution measurements from Laramie, Wyoming (41 N), using balloon-borne instruments, J. Geophys. Res., 108, 4167, doi:10.1029/2002JD002514, 2003. 4606

Eyring, V., Butchart, N., Waugh, D. W., Akiyoshi, H., Austin, J., Bekki, S., Bodeker, G. E., Boville, B. A., Brühl, C., Chipperfield, M. P., Cordero, E., Dameris, M., Deushi, M., Fioletov, V. E., Frith, S. M., Garcia, R. R., Gettelman, A., Giorgetta, M. A., Grewe, V., Jourdain, L., Kinnison, E., Mancini, E., Manzini, E., Marchand, M., Marsh, D. R., Nagashima, T., Newman, P. A., Nielsen, J. E., Pawson, S., Pitari, G., Plummer, D. A., Rozanov, E., Schraner, M., Shepherd, T. G., Shibata, K., Stolarski, R. S., Struthers, H., Tian, W., and Yoshiki, M.: Assessment of temperature, trace species, and ozone in chemistry-climate model simulations of the recent past, J. Geophys. Res., 111, D22308, doi:10.1029/2006JD007327, 2006. 4617, 4635

Gettelman, A., Hegglin, M. I., Son, S. W., Kim, J. H., Fujiwara, M., Birner, T., Kremser, S., Rex, M., Anel, J. A., Akiyoshi, H., Austin, J., Bekki, S., Braesike, P., Brühl, C., Butchart, N., Chipperfield, M., Dameris, M., Dhomse, S., Garny, H., Hardiman, S. C., Jöckel, P., Kinnison, D. E., Lamarque, J. F., Mancini, E., Marchand, M., Michou, M., Morgenstern, O., Pawson, S., Pitari, G., Plummer, D., Pyle, J. A., Rozanov, E., Scinocca, J., Shepherd, T. G., Shibata, K., Smale, D., Teyssèdre, H., and Tian, W.: Multimodel assessment of the upper troposphere and lower stratosphere: tropics and global trends, J. Geophys. Res, 115, D00M08, doi:10.1029/2009JD013638, 2010. 4604, 4618

Grainger, R. G., Lambert, A., Rodgers, C. D., Taylor, F. W., and Deshler, T.: Stratospheric aerosol effective radius, surface-area and volume estimated from infrared measurements, J. Geophys. Res. Atmos., 100, 16507–16518, 1995. 4608

Guo, S., Bluth, G. J. S., Rose, W. I., Watson, I. M., and Prata, A. J.: Re-evaluation of SO_2 release of the 15 June 1991 Pinatubo eruption using ultraviolet and infrared satellite sensors, Geochem. Geophy. Geosy., 5, Q04001, doi:10.1029/2003GC000654, 2004. 4606

Hervig, M. E., Russell, J. M., Gordley, L. L., Daniels, J., Drayson, S. R., and Park, J. H.: Aerosol effects and corrections in the Halogen Occultation Experiment, J. Geophys. Res., 100, 1067–1079, 1995. 4603

Kinnison, D. E., Grant, K. E., Connell, P. S., Rotman, D. A., and Wuebbles, D. J.: The chemical and radiative effects of the Mount-Pinatubo eruption, J. Geophys. Res. Atm., 99, 25705–25731, 1994. 4605

ACPD
13, 4601–4635, 2013

Labitzke, K. and McCormick, M. P.: Stratospheric temperature increases due to Pinatubo Aerosols, Geophys. Res. Lett., 19, 207–210, 1992. 4602
Lambert, A., Grainger, R. G., Remedios, J. J., Rodgers, C. D., Corney, M., and Taylor, F. W.: Measurements of the evolution of the Mt-Pinatubo aerosol cloud by ISAMS, Geophys. Res. Lett., 20, 1287–1290, 1993. 4606
Lambert, A., Grainger, R. G., Remedios, J. J., Reburn, W. J., Rodgers, C. D., Taylor, F. W., Roche, A. E., Kumer, J. B., Massie, S. T., and Deshler, T.: Validation of aerosol measurements from the improved stratospheric and mesospheric sounder, J. Geophys. Res., 101(D6), 9811–9830, doi:10.1029/95JD01702, 1996. 4603
Lambert, A., Grainger, R. G., Rodgers, C. D., Taylor, F. W., Mergenthaler, J. L., Kumer, J. B., and Massie, S. T.: Global evolution of the Mt. Pinatubo volcanic aerosols observed by the infrared limb-sounding instruments CLAES and ISAMS on the Upper Atmosphere Research Satellite, J. Geophys. Res. Atm., 102, 1495–1512, 1997. 4603, 4608
Lanzante, J. R. and Free, M.: Comparison of radiosonde and GCM vertical temperature trend profiles: effects of dataset choice and data homogenization, J. Climate, 21, p. 5417, 2007. 4604, 4617, 4618, 4635
Luo, B., Krieger, U. K., and Peter, T.: Densities and refractive indices of $H_2SO_4/HNO_3/H_2O$ solutions to stratospheric temperatures, Geophys. Res. Lett., 23, 3707–3710, doi:10.1029/96GL03581, 1996. 4613
McCormick, M. P.: Initial assessment of the stratospheric and climatic impact of the 1991 Mount-Pinatubo eruption – prologue, Geophys. Res. Lett., 19, 149–149, 1992. 4602
Mie, G.: Articles on the optical characteristics of turbid tubes, especially colloidal metal solutions, Ann. Phys., 25, 377–445, 1908. 4607, 4613
Minnis, P., Harrison, E. F., Stowe, L. L., Gibson, G. G., Denn, F. M., Doelling, D. R., and Smith, W. L.: Radiative climate forcing by the Mount-Pinatubo eruption, Science, 259, 1411–1415, 1993. 4602
Morgenstern, O., Giorgetta, M. A., Shibata K., Eyring, V., Waugh, D. W., Shepherd, T. G., Akiyoshi, H., Austin, J., Baumgaertner, A. J. G., Bekki, S., Braesicke, P., Brühl, C., Chipperfield, M. P., Cugnet, D., Dameris, M., Dhomse, S., Frith, S. M., Garny, H., Gettelman, A., Hardiman, S. C., Hegglin, M. I., Kinnison, D. E., Lamarque, J. F., Mancini, E., Manzini, E., Marchand, M., Michou, M., Nakamura, T., Nielsen, J. E., Pitari, G., Plummer, D. A., Rozanov, E., Scinocca, J. F., Smale, D., Teyssèdre, H., Toohey, M., Tian, W., and Yamashita, Y.: Review of the formulation of present generation stratospheric chemistry climate models and associ-

ACPD
13, 4601–4635, 2013

ated external forcings, J. Geophys. Res., 115, D00M02, doi:10.1029/2009JD013728, 2010. 4604, 4618

Rosen, J. M.: The vertical distribution of dust to 30 km, J. Geophys. Res., 69, 4673–4676, 1964. 4613

Russell, J. M., Gordley, L. L., Park, J. H., Drayson, S. R., Hesketh, W. D., Cicerone, R. J., Tuck, A. F., Frederick, J. E., Harries, J. E., and Crutzen, P. J.: The halogen occultation experiment, J. Geophys. Res., 98, 10777–10797, doi:10.1029/93JD00799, 1993. 4603

Russell, P. B., Livingston, J. M., Pueschel, R. F., Bauman, J. J., Pollack, J. B., Brooks, S. L., Hamill, P., Thomason, L. W., Stowe, L. L., Deshler, T., Dutton, E. G., and Bergstrom, R. W.: Global to microscale evolution of the Pinatubo volcanic aerosol derived from diverse measurements and analyses, J. Geophys. Res. Atm., 101, 18745–18763, 1996. 4605, 4609, 4612, 4613, 4614

Sato, M., Hansen, J. E., McCormick, M. P., and Pollack, J. B.: Stratospheric aerosol optical depths, 1850–1990, J. Geophys. Res. Atm., 98, 22987–22994, 1993. 4603, 4604, 4605, 4612, 4613, 4617, 4618

Schraner, M., Rozanov, E., Schnadt Poberaj, C., Kenzelmann, P., Fischer, A. M., Zubov, V., Luo, B. P., Hoyle, C. R., Egorova, T., Fueglistaler, S., Brönnimann, S., Schmutz, W., and Peter, T.: Technical Note: Chemistry-climate model SOCOL: version 2.0 with improved transport and chemistry/microphysics schemes, Atmos. Chem. Phys., 8, 5957–5974, doi:10.5194/acp-8-5957-2008, 2008. 4606, 4610, 4617

SPARC: Assessment of Stratospheric Aerosol Properties (ASAP), SPARC Report No. 4, edited by: Thomason, L. and Peter, T., World Climate Research Programme WCRP-124, WMO/TD No. 1295, 2006. 4603, 4604, 4605, 4606, 4609, 4612, 4617, 4618, 4619, 4620, 4628

SPARC-CCMVal, 2010: SPARC Report on the Evaluation of Chemistry-Climate Models, edited by: Eyring, V., Shepherd, T. G., and Waugh, D., Tech. rep., SPARC Report No. 5, WCRP-132, WMO/TD-No. 1526, WCRP-132, WMO/TD-No. 1526, 2010. 4604, 4617, 4618, 4635

Stenchikov, G. L., Kirchner, I., Robock, A., Graf, H. F., Antuna, J. C., Grainger, R. G., Lambert, A., and Thomason, L.: Radiative forcing from the 1991 Mount Pinatubo volcanic eruption, J. Geophys. Res. Atm, 103, 13837–13857, 1998. 4603, 4604, 4605, 4610, 4612, 4617, 4618, 4619

Stowe, L. L., Carey, R. M., and Pellegrino, P. P.: Monitoring the Mt-Pinatubo aerosol layer with NOAA-11 AVHRR data, Geophys. Res. Lett., 19, 159–162, 1992. 4602

ACPD
13, 4601–4635, 2013

Thomason, L. W.: Observations of a new SAGE-II aerosol extinction mode following the eruption of Mt-Pinatubo, Geophys. Res. Lett., 19, 2179–2182, 1992. 4602

Thomason, L. W., Kent, G. S., Trepte, C. R., and Poole, L. R.: A comparison of the stratospheric aerosol background periods of 1979 and 1989–1991, J. Geophys. Res. Atm., 102, 3611–3616, 1997a. 4610

Thomason, L. W., Poole, L. R., and Deshler, T.: A global climatology of stratospheric aerosol surface area density deduced from Stratospheric Aerosol and Gas Experiment II measurements: 1984–1994, J. Geophys. Res. Atm, 102, 8967–8976, 1997b. 4606, 4609

Thomason, L. W.: Toward a combined SAGE II-HALOE aerosol climatology: an evaluation of HALOE version 19 stratospheric aerosol extinction coefficient observations, Atmos. Chem. Phys., 12, 8177–8188, doi:10.5194/acp-12-8177-2012, 2012. 4603

Weisenstein, D. K., Yue, G. K., Ko, M. K. W., Sze, N. D., Rodriguez, J. M., and Scott, C. J.: A two-dimensional model of sulfur species and aerosols, J. Geophys. Res. Atmos., 102, 13019–13035, 1997. 4605

Wurl, D., Grainger, R. G., McDonald, A. J., and Deshler, T.: Optimal estimation retrieval of aerosol microphysical properties from SAGE II satellite observations in the volcanically unperturbed lower stratosphere, Atmos. Chem. Phys., 10, 4295–4317, doi:10.5194/acp-10-4295-2010, 2010. 4605

ACPD
13, 4601–4635, 2013

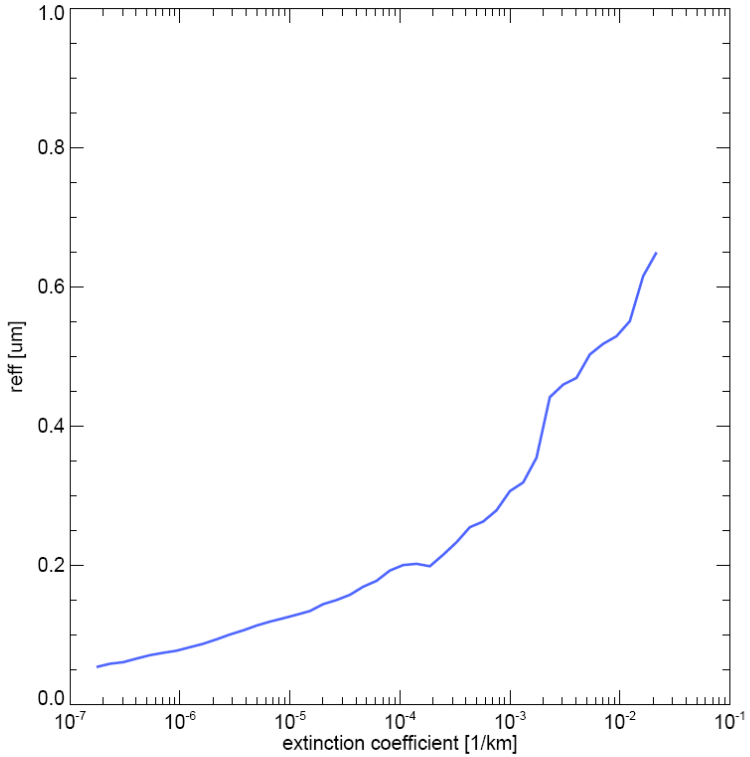

Fig. 1. Effective radii (µm) derived from the SAGE_4λ first step versus extinction coefficients at 1.024 µm from SAGE II. Black dots and red dots represent values within and outside one standard deviation, respectively. Dashed blue line represents the median values.

ACPD
13, 4601–4635, 2013

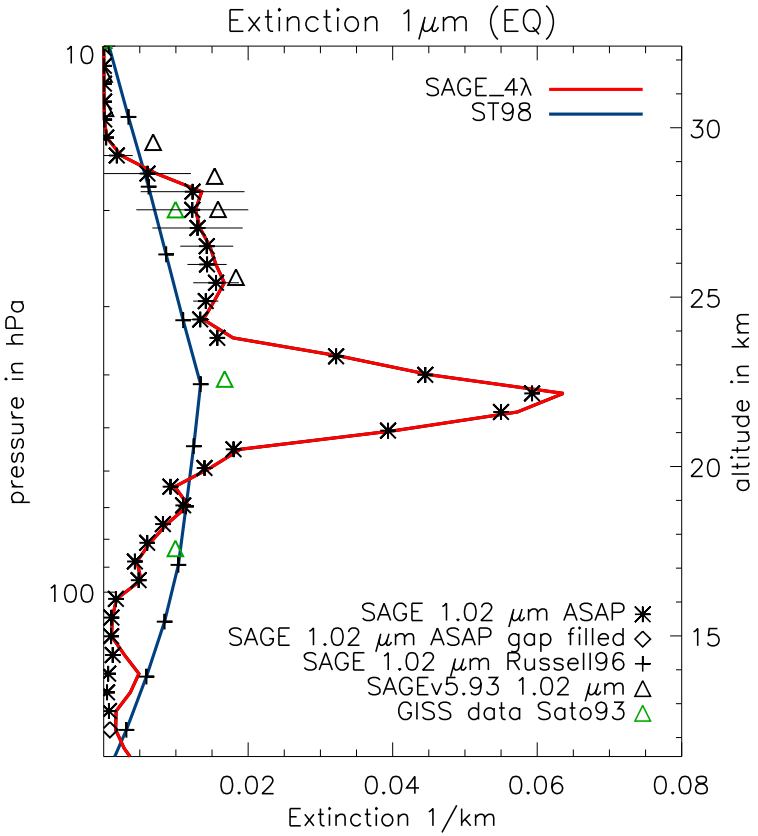

Fig. 2. Zonal mean extinction for August 1991 at 1.024 µm at the equator. Horizontal lines show standard deviations of SAGE ASAP measurements.

ACPD
13, 4601–4635, 2013

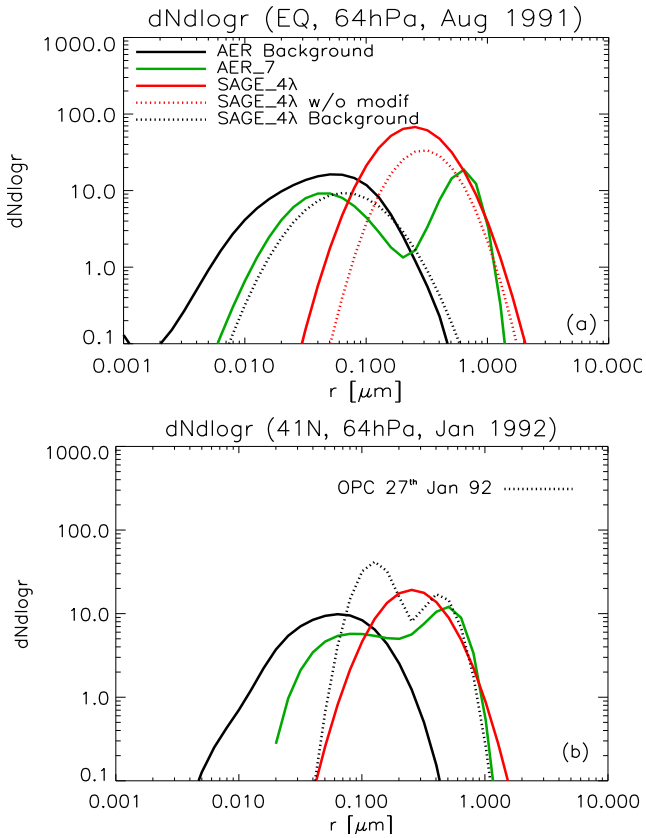

Fig. 3. Differential number density dN/d log r as a function of aerosol radius at 64 hPa for **(a)** the equator (5° S–5° N) in August 1991, and **(b)** northern mid-latitudes (40° N) in January 1992. SAGE_4λ background size distribution is represented by the January 1991 background conditions. Dashed black line in **(b)** shows the OPC measurements at Laramie, Wyoming (41° N).

ACPD
13, 4601–4635, 2013

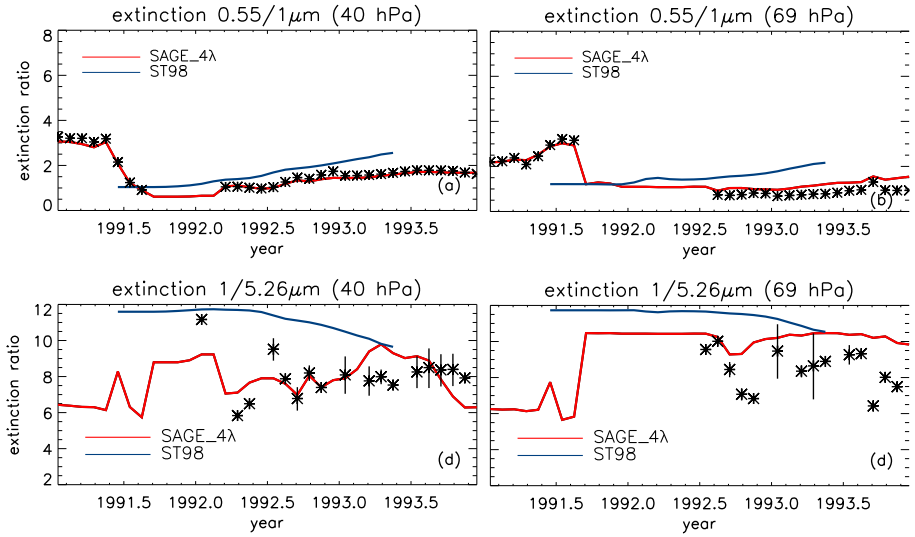

Fig. 4. Extinction ratio of 0.525 µm/1.024 µm **(a, b)** and 1 µm/5.26 µm **(c, d)**. At the equator at 40 hPa altitude **(a, c)** and at 69 hPa altitude **(b, d)**. Asterisks in **(a, b)** show ratio of SAGE II 0.525 µm/1.024 µm (SPARC, 2006) and asterisks in **(c, d)** show ratio of SAGE II 1.024 µm and HALOE 5.26 µm.

ACPD
13, 4601–4635, 2013

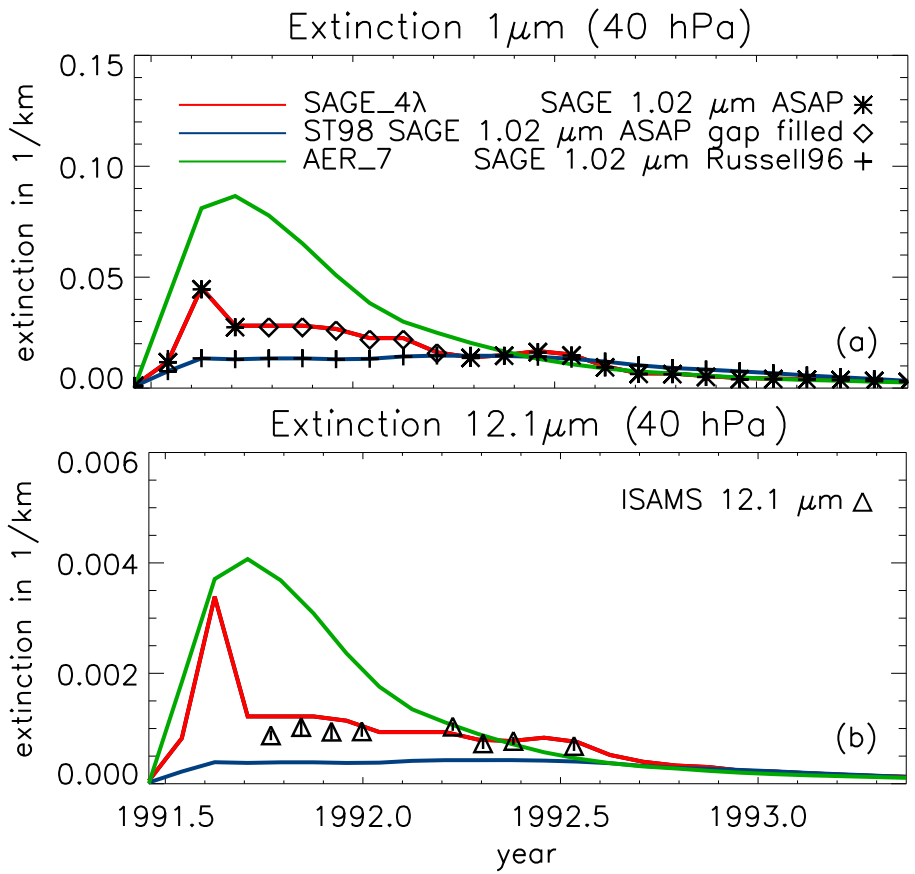

Fig. 5. Zonal mean 40 hPa extinction from June 1991 to June 1993 for 1.024 µm **(a)** and 12.1 µm **(b)** at 5° S–5° N. Vertical lines show standard deviations of SAGE ASAP measurements and the random error estimation+standard deviation for the ISAMS measurements.

ACPD
13, 4601–4635, 2013

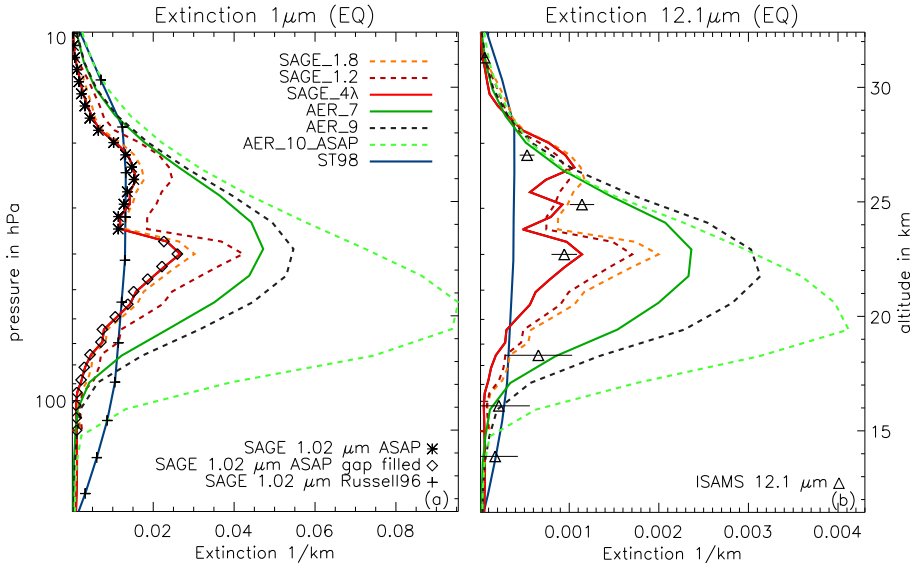

Fig. 6. Zonal mean extinction for December 1991 at 1.024 µm and 12.1 µm at 5° S–5° N. Horizontal lines show standard deviations for the SAGE ASAP measurements and the random error estimation+standard deviation for the ISAMS measurements.

ACPD
13, 4601–4635, 2013

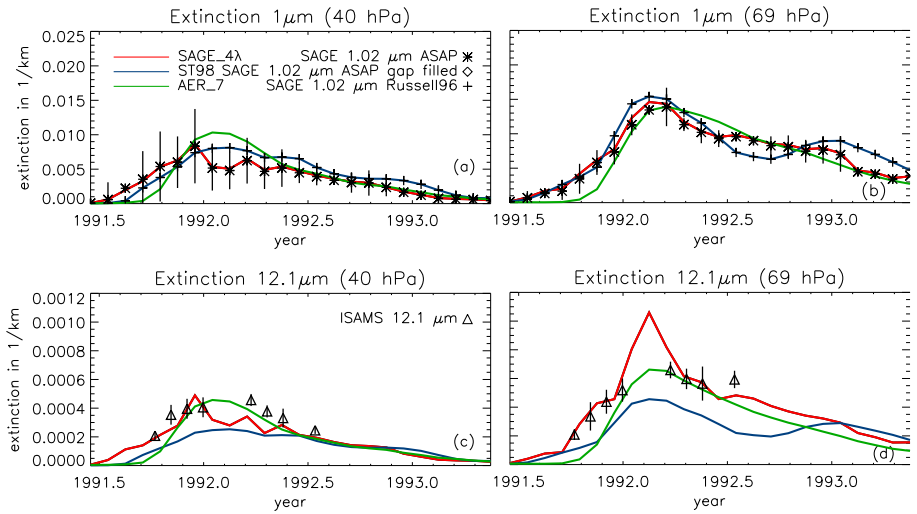

Fig. 7. Zonal mean extinction from June 1991 to June 1993 for 1.024 µm and 12.1 µm at 30°–40° N. Left column at 40 hPa, right column at 69 hPa. Vertical lines show standard deviations of SAGE ASAP measurements and the random error estimation+standard deviation for the ISAMS measurements.

ACPD
13, 4601–4635, 2013

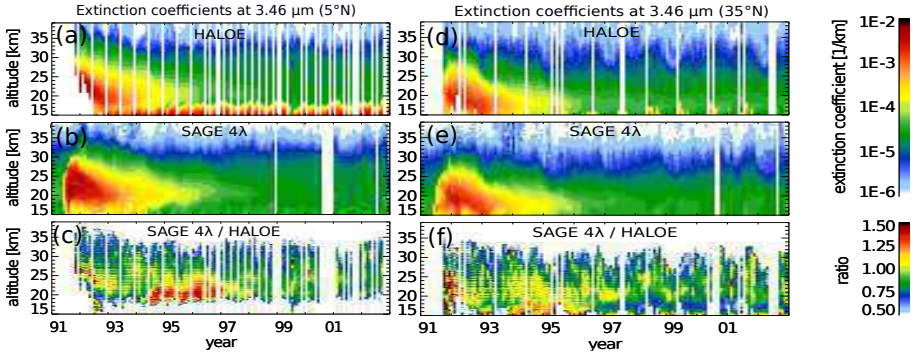

Fig. 8. HALOE 5° N extinction coefficients at 3.46 µm **(a)**. Calculated 5° N extinction coefficients at 3.46 µm using the 4l-size distribution **(b)**. Ratio of the 4l-extinction coefficients to HALOE measurements **(c)**. HALOE 35° N extinction coefficients at 3.46 µm **(d)**. Calculated 35° N extinction coefficients at 3.46 µm using the 4l-size distribution **(e)**. Ratio of the 4l-extinction coefficients to HALOE measurements **(f)**.

ACPD
13, 4601–4635, 2013

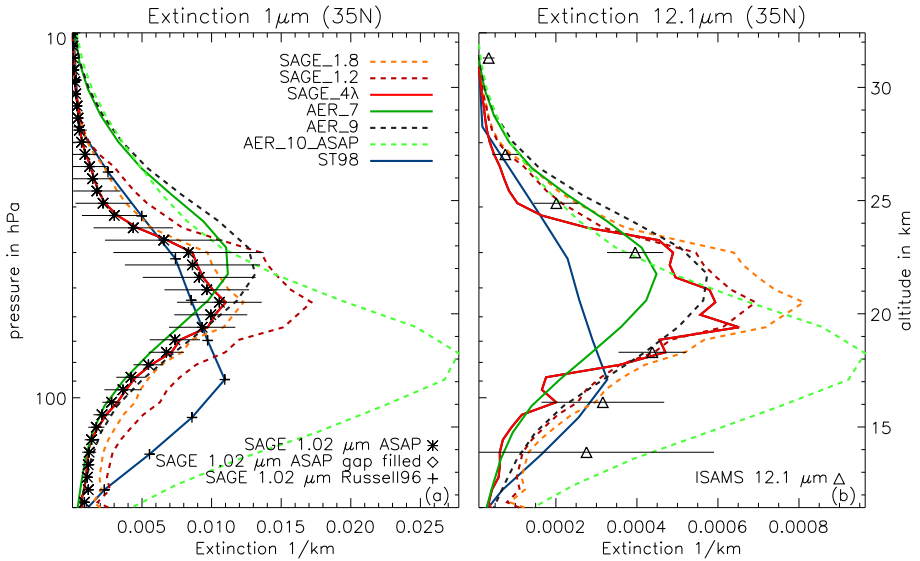

Fig. 9. Zonal mean extinction for December 1991 at 1.024 µm and 12.1 µm at 30–40° N. Horizontal lines show standard deviations of SAGE ASAP measurements and the random error estimation+standard deviation for the ISAMS measurements.

ACPD
13, 4601–4635, 2013

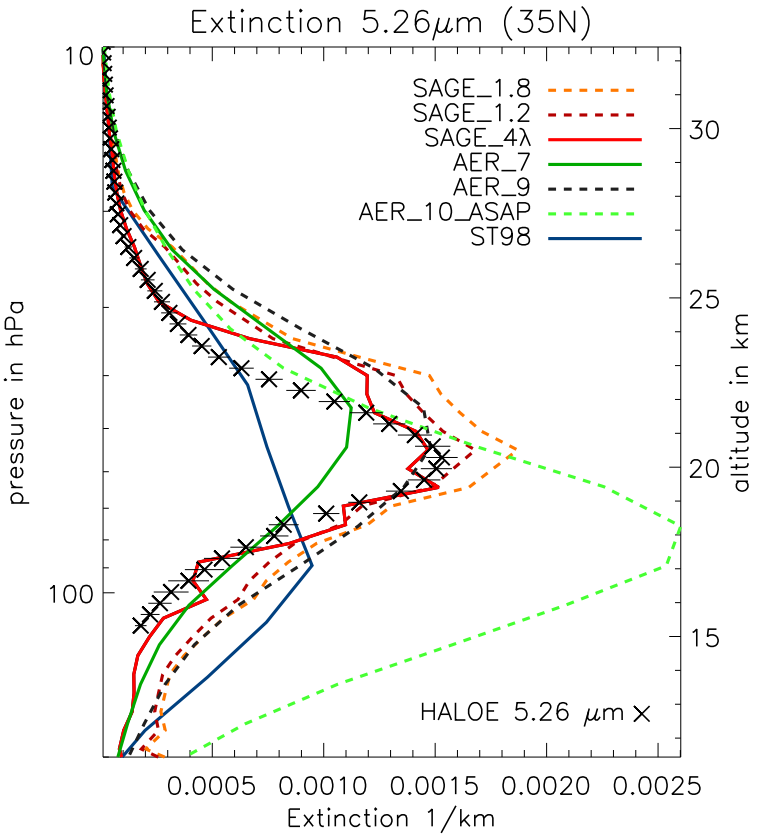

Fig. 10. Zonal mean extinction for December 1991 at 5.26 µm at 30–40° N. Horizontal lines show standard deviations of HALOE measurements.

ACPD
13, 4601–4635, 2013

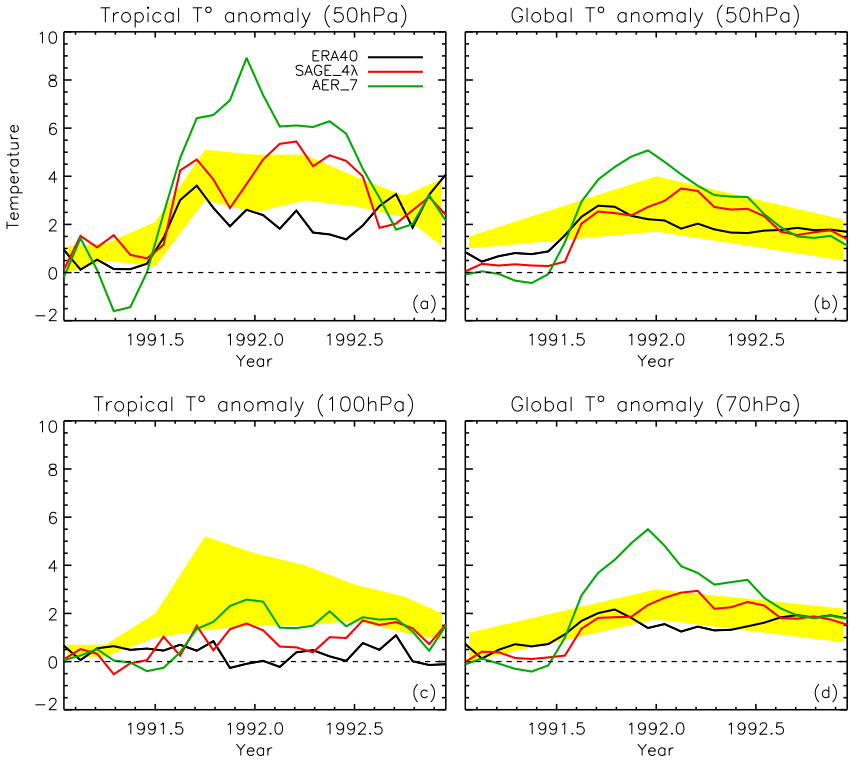

Fig. 11. Zonal mean temperature anomalies from SOCOL for tropics (20° S–20° N) at 50 hPa **(a)** and 100 hPa **(c)** as well as global mean anomaly at 50 hPa **(b)** and 70 hPa **(d)**. Scenarios anomalies (SAGE_4λ and AER_7) are computed with respect to a control simulation. Black line represents ERA-40 temperature anomalies with respect to 1995–1999. Shadings display approximate anomaly ranges calculated by general circulation models as examined in Lanzante and Free (2007) for **(a, c)** and by chemistry climate models as examined in Eyring et al. (2006) in **(b)** and SPARC-CCMVal (2010) in **(d)**.

ACPD
13, 4601–4635, 2013